

Transient Nonlinear Electrothermal Adjoint Sensitivity Analysis for HVDC Cable Joints

^{1,2}M. Greta Ruppert, ^{1,2}Yvonne Späck-Leigsnering,
^{1,2}Herbert De Gersem

¹ *Technische Universität Darmstadt, Institute for Accelerator Science and Electromagnetic Fields, Schlossgartenstr. 8, 64289 Darmstadt, Germany*

² *Technische Universität Darmstadt, Graduate School of Computational Engineering Dolivostraße 15, 64293 Darmstadt, Germany*

Abstract Efficient computation of sensitivities is a promising approach for efficiently designing and optimizing high voltage direct current cable joints. This paper presents the adjoint variable method for coupled nonlinear transient electrothermal problems as an efficient approach to compute sensitivities with respect to a large number of design parameters. The method is used to compute material sensitivities of a 320 kV high voltage direct current cable joint specimen. The results are validated against sensitivities obtained via the direct sensitivity method.

1 Introduction

Cable joints are known to be the most vulnerable components of high voltage direct current (HVDC) cable systems as they suffer from high internal electric field stresses [1, 2, 3, 4]. One solution to mitigate these stresses is the integration of a layer of nonlinear field grading material (FGM) [5, 6]. This material becomes highly conductive in areas of high stress, effectively reducing electric field stress and redistributing voltage drop to lower-stress areas.

Recent developments in material science allow for the customization of an FGM's nonlinear conductivity, enabling more precise designs to fit specific applications [7, 6]. In addition to practical know-how, finite element (FE) simulations play an increasingly vital role for the development of FGMs. However, only few studies systematically investigated the various design parameters of FGMs [6, 5, 8, 9].

One way to study the influence of individual design parameters without extensive parameter sweeps is the use of sensitivities, i.e. gradients. Sensitivities provide insights on the impact of small changes in a design parameter on a quantity of interest (QoI), and allow an efficient optimization of FGMs [10].

Different methods for sensitivity computation exist. Commonly used methods like, e.g., finite differences and the direct sensitivity method, have the drawback that their computational costs scale linearly with the number of parameters [11, 12]. The adjoint variable method, on the other hand, features computational costs that are nearly unaffected by the number of parameters [11, 13, 12]. In high voltage engineering, the adjoint variable method has recently been formulated for linear electroquasistatic (EQS) problems in frequency domain [14], nonlinear EQS problems in the time domain [15], and stationary nonlinear coupled electrothermal problems [16]. However, for an investigation of the electrothermal behavior of a cable joint during transient overvoltages, a fully coupled transient electroquasistatic-thermal (EQST) analysis is required [17, 18, 19]. This study formulates and numerically solves the adjoint variable method for transient coupled EQST problems with nonlinear material properties. The method is implemented within the Python-based FE framework *Pyrit* [20] and applied to the model of a 320 kV HVDC cable joint under switching impulse operation. The method is validated using results obtained via the direct sensitivity method as a reference. Moreover, the benefits of a multi-rate time-integration approach are demonstrated. The outcome of the paper is an FE-based adjoint sensitivity analysis tool incorporating electrothermal multiphysics, nonlinear

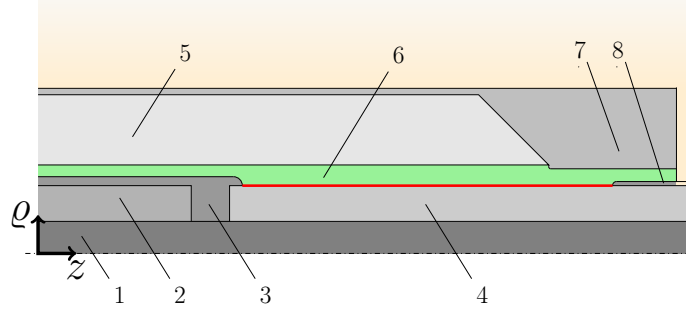


Figure 1: Schematic of the investigated HVDC cable joint [5] in a cylindrical coordinate system (ρ, z) . The numbers indicate the different materials as described in the text, the FGM layer is highlighted in green. The red line marks the interface between the FGM layer and the cable insulation. The cable joint is surrounded by a 30 cm thick layer of sand and buried 2 m beneath the ground.

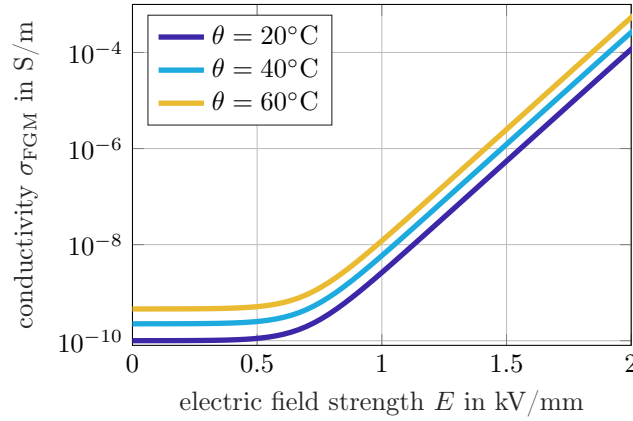


Figure 2: Nonlinear field- and temperature-dependent conductivity of the FGM. The FGM conductivity is modeled by the analytic function (1).

material properties and transient overvoltages, which are the three challenges to be tackled in cable joint design.

2 Modeling and Numerical Approach

2.1 Cable Joint Specimen

Figure 1 shows a cut of the investigated 320 kV HVDC cable joint model [5]. The cable joint connects two cables segments, each consisting of a copper conductor (domain 1), an insulation layer (domain 4) and a grounded outer sheath (domain 8). The conductors are connected by an aluminum connector (domain 2), which is encased in conductive silicone rubber (SiR) (domain 3). The primary insulation of the cable (domain 4) is composed of cross-linked polyethylene (XLPE), while the main insulation of the cable joint body (domain 5) is made from insulating SiR. The outer sheath of the cable joint (domain 7) as well as the outer semiconductor of the cable (domain 8) are grounded. The cable joint is surrounded by a 30 cm thick layer of sand and buried 2 m beneath the ground.

In the simulation, a switching impulse overvoltage is applied to the domains 1 to 3, which are modeled as perfect electric conductors (PECs) due to their substantially higher conductivities relative to the insulating materials. The assumed operating temperatures are 65°C at the copper conductors and 20°C for the ambient temperature at the top of the soil layer [9]. For a detailed description of the geometric measurements of the cable joint and material characteristics, see [9, 5].

To mitigate harmful electric field stresses at the insulation interfaces between the XLPE and SiR, a layer of nonlinear FGM (domain 6) is introduced. This FGM layer dynamically adjusts its conductivity based on the local electric field strength, E . In regions of high electric field stress, the FGM's conductivity increases, thereby redistributing the electric field by shifting the voltage drop to

less stressed areas. This results in a more balanced electric field distribution across the insulation layers.

The nonlinear conductivity of the FGM, σ_{FGM} , is modeled by the following function [5]:

$$\sigma_{\text{FGM}}(E, \theta) = p_1 \frac{1 + p_4^{(E-p_2)p_2^{-1}}}{1 + p_4^{(E-p_3)p_2^{-1}}} \exp(-p_5(\theta^{-1} - \theta_0^{-1})), \quad (1)$$

where θ is the temperature, $\theta_0 = 293.15 \text{ K}$ is the reference ambient temperature, and p_1 to p_5 are design parameters. Selecting suitable values for p_1 to p_5 is a non-trivial task, as each parameter significantly influences the FGM's nonlinear field-grading behavior. For example, p_1 determines the baseline conductivity, while p_2 specifies the electric field strength where the FGM transitions from baseline to nonlinear response. In this study, the parameters are initially set to $p_1 = 10^{-10} \text{ S/m}$, $p_2 = 0.7 \text{ kV/m}$, $p_3 = 2.4 \text{ kV/m}$, $p_4 = 1864$ and $p_5 = 3713.59 \text{ K}$, with the field dependence at a fixed temperature illustrated in Fig. 2.

2.2 Electrothermal Modeling

The capacitive-resistive-thermal behavior of a cable joint that is subjected to transient overvoltages, e.g. a lightning strike or switching operations, can be described by the combination of the transient EQS equation and the transient heat conduction equation [21]. The transient EQS problem reads

$$\text{div}(\mathbf{J} + \partial_t \mathbf{D}) = 0, \quad t \in [t_s, t_f], \quad \mathbf{r} \in \Omega; \quad (2a)$$

$$\phi = \phi_D, \quad t \in [t_s, t_f], \quad \mathbf{r} \in \Gamma_{D,\text{el}}; \quad (2b)$$

$$(\mathbf{J} + \partial_t \mathbf{D}) \cdot \mathbf{n}_{\text{el}} = 0, \quad t \in [t_s, t_f], \quad \mathbf{r} \in \Gamma_{N,\text{el}}; \quad (2c)$$

$$\phi = \phi_0, \quad t = t_s, \quad \mathbf{r} \in \Omega, \quad (2d)$$

where \mathbf{J} is the resistive current density, \mathbf{D} is the electric displacement field, \mathbf{E} is the electric field and ϕ is the electric scalar potential. σ represents the electric conductivity and ε represents the electric permittivity. \mathbf{r} and Ω denote the spatial coordinate and the computational domain in space, respectively. t is the time and t_s and t_f denote the initial and final simulation time, respectively. ϕ_D are the fixed voltages at the Dirichlet boundaries, $\Gamma_{D,\text{el}} \neq \emptyset$. The Neumann boundaries are denoted as $\Gamma_{N,\text{el}} = \partial\Omega \setminus \Gamma_{D,\text{el}}$. ϕ_0 denotes the initial condition of the electric potential, i.e. the steady state potential distribution before the transient event.

The transient heat conduction equation reads

$$\partial_t(c_V \theta) + \text{div}(\dot{\mathbf{q}}) = \dot{q}_{\text{Joule}}, \quad t \in [t_s, t_f], \quad \mathbf{r} \in \Omega; \quad (3a)$$

$$\theta = \theta_D, \quad t \in [t_s, t_f], \quad \mathbf{r} \in \Gamma_{D,\text{th}}; \quad (3b)$$

$$\dot{\mathbf{q}} \cdot \mathbf{n}_{\text{th}} = 0, \quad t \in [t_s, t_f], \quad \mathbf{r} \in \Gamma_{N,\text{th}}; \quad (3c)$$

$$\theta = \theta_0, \quad t = t_s, \quad \mathbf{r} \in \Omega, \quad (3d)$$

where $\dot{\mathbf{q}} = -\lambda \text{grad}(\theta)$ is the heat flux density, c_V is the volumetric heat capacity and λ is the thermal conductivity. θ_0 denotes the initial condition of the temperature. θ_D are the fixed temperatures at the Dirichlet boundaries, $\Gamma_{D,\text{th}} \neq \emptyset$. At the Neumann boundaries, $\Gamma_{N,\text{th}} = \partial\Omega \setminus \Gamma_{D,\text{th}}$, the normal heat flux density is set to zero. The two equations are coupled along the Joule losses, $\dot{q}_{\text{Joule}} = \mathbf{J} \cdot \mathbf{E}$, and possible temperature dependencies of electric materials, e.g., the FGM conductivity defined in (1).

2.3 Discretization in Space and Time

The electrothermal behavior of the cable joint is formulated as a two-dimensional (2D) axisymmetric FE problem. The electric scalar potential and the temperature are discretized by

$$\phi(\mathbf{r}, t) \approx \sum_r u_r(t) N_r(\mathbf{r}), \quad (4a)$$

$$\theta(\mathbf{r}, t) \approx \sum_r v_r(t) N_r(\mathbf{r}) \quad (4b)$$

where N_r are linear nodal FE shape functions and u_r and v_r are the degrees of freedom, which are assembled in the vectors \mathbf{u} and \mathbf{v} , respectively. The semi-discrete versions according to the Ritz-Galerkin procedure of (2) and (3) read

$$\mathbf{K}_\sigma \mathbf{u} + \partial_t (\mathbf{K}_\varepsilon \mathbf{u}) = 0, \quad (5a)$$

$$\mathbf{K}_\lambda \mathbf{v} + \partial_t (\mathbf{M}_{cV} \mathbf{v}) = \mathbf{s}_{\dot{q}_{\text{Joule}}}, \quad (5b)$$

with

$$[\mathbf{K}(\cdot)]_{rs} = \int_{\Omega} (\cdot) \text{grad}(N_r) \cdot \text{grad}(N_s) \, d\Omega; \quad (6a)$$

$$[\mathbf{M}(\cdot)]_{rs} = \int_{\Omega} (\cdot) N_r N_s \, d\Omega; \quad ; \quad (6b)$$

$$[\mathbf{s}(\cdot)]_r = \int_{\Omega} (\cdot) N_r \, d\Omega; \quad . \quad (6c)$$

The model is implemented for axisymmetric problems in the freely available FE framework *Pyrit* [20]. The integrals (6a)–(6c) are carried out on a triangular mesh of the cut shown in Fig. 1, i.e., $d\Omega = 2\pi \rho d\rho dz$. The matrices are assembled for $r, s = 1, \dots, N_{\text{node}}$, where N_{node} denotes the number of nodes of the mesh. A weak multi-rate coupling scheme (see Fig. 3) [22] with implicit Euler time-stepping is performed. The nonlinearity arising in the electric subproblem (5a) due to the FGM is solved using the Newton method.

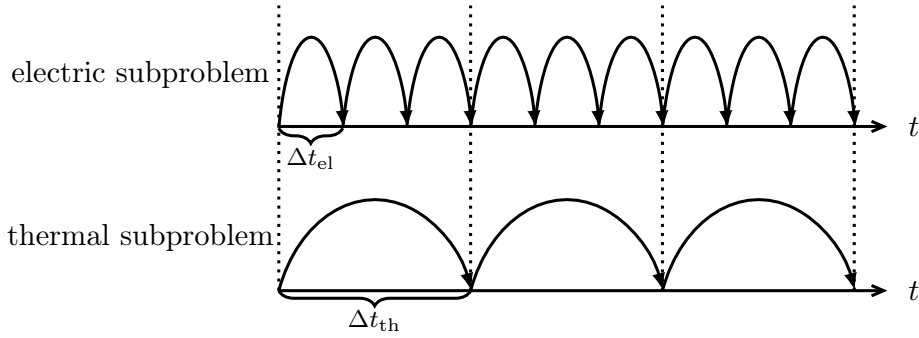


Figure 3: Illustration of the weak multi-rate coupling scheme: With thermal dynamics spanning minutes to hours and electric phenomena occurring on the microsecond to millisecond scale, distinct time step sizes are adopted for the electric and thermal subproblems. The thermal time step, Δt_{th} , is set as a multiple of the smaller electric time step, Δt_{el} . As indicated by the dotted lines, the field distributions are exchanged between both subproblems after each thermal time step.

3 Sensitivities of Cable Joint Materials

As shown in Sec. 2.1, the nonlinear conductivity curve of an FGM is represented as an analytical function shaped by various design parameters, denoted as $\mathbf{p} = [p_1, \dots, p_{N_p}]$. When designing an FGM, the quality of the nonlinear conductivity curve is evaluated based on a number of QoIs, G_k , $k = 1, \dots, N_{\text{QoI}}$, such as the Joule losses or the electric field at critical positions [6, 5]. The design process, i.e. the optimization of \mathbf{p} , can be accelerated by using sensitivity information [10]. Sensitivities quantify the influence of small changes in a design parameter, p_j , on a given QoI, G_k , expressed as $\frac{dG_k}{dp_j}(\mathbf{p}_0)$, where \mathbf{p}_0 represents the current parameter configuration. In this section, it is discussed how sensitivities of HVDC cable joint materials can be computed most effectively.

3.1 Direct Sensitivity Method

One of the most frequently used methods for sensitivity computation is the direct sensitivity method (DSM). The DSM appeals with its simple derivation and uncomplicated implementation. It is based on the derivatives of (2) and (3) to p_j , from which the derivatives of the electric potential and the

temperature to p_j can be computed, i.e. $\frac{d\phi}{dp_j}(\mathbf{p}_0)$, and $\frac{d\theta}{dp_j}(\mathbf{p}_0)$. The sensitivity can then be calculated directly using the chain rule:

$$\frac{dG_k}{dp_j}(\mathbf{p}_0) = \frac{\partial G_k}{\partial p_j}(\mathbf{p}_0) + \frac{\partial G_k}{\partial \phi} \frac{d\phi}{dp_j}(\mathbf{p}_0) + \frac{\partial G_k}{\partial \theta} \frac{d\theta}{dp_j}(\mathbf{p}_0). \quad (7)$$

Since this process has to be repeated for each parameter, p_1, \dots, p_{N_P} , the DSM requires the solution of N_P individually coupled systems of linear partial differential equations (PDEs) in addition to the nominal solution. Consequently, for large numbers of parameters, the DSM leads to prohibitively long simulation times.

3.2 Adjoint Variable Method

An alternative approach for sensitivity computation is the adjoint variable method (AVM). The AVM is very efficient when the number of parameters, N_P , is greater than the number of quantities of interest (QoIs), N_{QoI} . It has originally been applied for the analysis of electric networks and only recently gained interest in the high voltage (HV) engineering community [14, 16, 15]. In this paper, the method is adapted for the *transient coupled electrothermal* analysis of HVDC cable joints.

The AVM avoids the computation of $\frac{d\phi}{dp_j}(\mathbf{p}_0)$ and $\frac{d\theta}{dp_j}(\mathbf{p}_0)$ for each parameter by a clever representation of the QoIs: Each QoI, G_k , is formulated as an integral over the computational domain in space and time, $\Omega \times [t_s, t_f]$, by means of a functional, g_k . Furthermore, the EQS equation (2) and the transient heat conduction equation (3) are added, multiplied by test functions $w_{el,k}$ and $w_{th,k}$, respectively as additional terms:

$$\begin{aligned} G_k(\phi, \theta, \mathbf{p}) &= \int_{\Omega} \int_{t_s}^{t_f} g_k(\phi, \theta, \mathbf{r}, t, \mathbf{p}) dt d\Omega \\ &\quad - \int_{\Omega} \int_{t_s}^{t_f} w_{el,k}(\mathbf{r}, t) \underbrace{(\operatorname{div}(\partial_t \mathbf{D} + \mathbf{J}))}_{\text{Eq. (2a)}_0} dt d\Omega \\ &\quad - \int_{\Omega} \int_{t_s}^{t_f} w_{th,k}(\mathbf{r}, t) \underbrace{(\partial_t(c_V \theta) + \operatorname{div}(\dot{\mathbf{q}}) - \dot{q}_{\text{Joule}})}_{\text{Eq. (3a)}_0} dt d\Omega. \end{aligned} \quad (8)$$

As indicated by the curved brackets, the additional terms are zero by construction. Consequently, the test functions, $w_{el,k}$ and $w_{th,k}$, can be chosen freely without changing the value of the QoIs. Taking the derivative of (8) to p_j yields:

$$\begin{aligned} \frac{dG_k}{dp_j}(\mathbf{p}_0) &= \int_{\Omega} \int_{t_s}^{t_f} \frac{\partial g_k}{\partial p_j}(\mathbf{p}_0) dt d\Omega + \int_{\Omega} \int_{t_s}^{t_f} \frac{\partial g_k}{\partial \phi} \frac{d\phi}{dp_j}(\mathbf{p}_0) + \frac{\partial g_k}{\partial \theta} \frac{d\theta}{dp_j}(\mathbf{p}_0) dt d\Omega \\ &\quad - \int_{\Omega} \int_{t_s}^{t_f} w_{el,k}(\mathbf{r}, t) \cdot f_{el} \left(\frac{d\phi}{dp_j}, \frac{d\theta}{dp_j}, \mathbf{r}, t, \mathbf{p}_0 \right) dt d\Omega \\ &\quad - \int_{\Omega} \int_{t_s}^{t_f} w_{th,k}(\mathbf{r}, t) \cdot f_{th} \left(\frac{d\phi}{dp_j}, \frac{d\theta}{dp_j}, \mathbf{r}, t, \mathbf{p}_0 \right) d\Omega dt, \end{aligned} \quad (9)$$

where f_{el} and f_{th} are the derivatives of (2a) and (3a) to p_j , respectively, i.e.

$$f_{el} = \frac{d}{dp_j} (\operatorname{div}(\partial_t \mathbf{D} + \mathbf{J}))(\mathbf{p}_0), \quad (10a)$$

$$f_{th} = \frac{d}{dp_j} (\partial_t(c_V \theta) + \operatorname{div}(\dot{\mathbf{q}}) - \dot{q}_{\text{Joule}})(\mathbf{p}_0). \quad (10b)$$

Equation (9) shows that the test functions are multiplied by factors containing $\frac{d\phi}{dp_j}(\mathbf{p}_0)$ and $\frac{d\theta}{dp_j}(\mathbf{p}_0)$. The idea of the AVM is to choose the test functions in such a way that all occurrences of these unwanted terms vanish. This is achieved by choosing the test functions as the solutions of the so-called adjoint problem [11, 13]. The adjoint problem for nonlinear coupled EQST problems with parameter-dependent materials, i.e., $\sigma(\mathbf{E}, \theta, \mathbf{p})$, $\varepsilon(\mathbf{E}, \theta, \mathbf{p})$, $\lambda(\theta, \mathbf{p})$, $c_V(\theta, \mathbf{p})$, reads:

$$\operatorname{div} \left(\bar{\varepsilon}_d \frac{\partial}{\partial t} \operatorname{grad}(w_{el,k}) \right) - \operatorname{div}(\bar{\sigma}_d \operatorname{grad}(w_{el,k}))$$

$$+ \operatorname{div} (w_{\text{th},k} (\bar{\sigma}_d \mathbf{E} + \mathbf{J})) = \frac{\partial g_k}{\partial \phi}, \quad t \in [t_s, t_f], \quad \mathbf{r} \in \Omega; \quad (11a)$$

$$w_{\text{el},k} = 0 \quad , \quad t \in [t_s, t_f], \quad \mathbf{r} \in \Gamma_{\text{D,el}}; \quad (11b)$$

$$\left(-\bar{\sigma}_d \operatorname{grad} (w_{\text{el},k}) + \bar{\varepsilon}_d \frac{\partial}{\partial t} \operatorname{grad} (w_{\text{el},k}) + w_{\text{th},k} (\bar{\sigma}_d \mathbf{E} + \mathbf{J}) \right) \cdot \mathbf{n}_{\text{el}} = 0 \quad , \quad t \in [t_s, t_f], \quad \mathbf{r} \in \Gamma_{\text{N,el}}; \quad (11c)$$

$$w_{\text{el},k} = 0 \quad , \quad t = t_f \quad , \quad \mathbf{r} \in \Omega, \quad (11d)$$

and

$$\begin{aligned} & \frac{\partial}{\partial t} \operatorname{grad} (w_{\text{el},k}) \cdot \frac{\partial \varepsilon}{\partial \theta} \mathbf{E} - \operatorname{grad} (w_{\text{el},k}) \cdot \frac{\partial \sigma}{\partial \theta} \mathbf{E} \\ & - \frac{\partial w_{\text{th},k}}{\partial t} \left(c_V + \frac{\partial c_V}{\partial \theta} \theta \right) - \operatorname{div} (\lambda \operatorname{grad} (w_{\text{th},k})) \\ & + \operatorname{grad} (w_{\text{th},k}) \cdot \frac{\partial \lambda}{\partial \theta} \operatorname{grad} (\theta) - w_{\text{th},k} \frac{\partial \sigma}{\partial \theta} E^2 = \frac{\partial g_k}{\partial \theta}, \quad t \in [t_s, t_f], \quad \mathbf{r} \in \Omega; \end{aligned} \quad (12a)$$

$$w_{\text{th},k} = 0 \quad , \quad t \in [t_s, t_f], \quad \mathbf{r} \in \Gamma_{\text{D,th}}; \quad (12b)$$

$$-\lambda \operatorname{grad} (w_{\text{th},k}) \cdot \mathbf{n}_{\text{th}} = 0 \quad , \quad t \in [t_s, t_f], \quad \mathbf{r} \in \Gamma_{\text{N,th}}; \quad (12c)$$

$$w_{\text{th},k} = 0 \quad , \quad t = t_f \quad , \quad \mathbf{r} \in \Omega, \quad (12d)$$

where all quantities are evaluated at the currently implemented parameter configuration, \mathbf{p}_0 . Moreover, $\bar{\sigma}_d$ and $\bar{\varepsilon}_d$ denote the differential electric conductivity and differential permittivity, respectively, i.e. [15, 23]

$$\begin{aligned} \bar{\sigma}_d(\mathbf{E}, \theta) &= \sigma(\mathbf{E}, \theta) \begin{bmatrix} 1 & 0 \\ 0 & 1 \end{bmatrix} + 2 \frac{d\sigma}{dE^2}(\mathbf{E}, \theta) \mathbf{E} \mathbf{E}^T, \\ \bar{\varepsilon}_d(\mathbf{E}, \theta) &= \varepsilon(\mathbf{E}, \theta) \begin{bmatrix} 1 & 0 \\ 0 & 1 \end{bmatrix} + 2 \frac{d\varepsilon}{dE^2}(\mathbf{E}, \theta) \mathbf{E} \mathbf{E}^T, \end{aligned}$$

and are evaluated for the operating points defined by the nominal solution. Once the electric potential, the temperature and the test functions are available, the sensitivity with respect to any parameter can be computed directly by

$$\begin{aligned} \frac{dG_k}{dp_j}(\mathbf{p}_0) &= \int_{t_s}^{t_f} \int_{\Omega} \frac{\partial g}{\partial p_j} d\Omega dt \\ &+ \int_{t_s}^{t_f} \int_{\Omega} \operatorname{grad} (w_{\text{el},k}) \cdot \frac{\partial \sigma}{\partial p_j} \mathbf{E} d\Omega dt \\ &- \int_{t_s}^{t_f} \int_{\Omega} \frac{\partial}{\partial t} \operatorname{grad} (w_{\text{el},k}) \cdot \frac{\partial \varepsilon}{\partial p_j} \mathbf{E} d\Omega dt \\ &+ \int_{t_s}^{t_f} \int_{\Omega} \frac{\partial w_{\text{th},k}}{\partial t} \frac{\partial c_V}{\partial p_j} \theta d\Omega dt \\ &+ \int_{t_s}^{t_f} \int_{\Omega} w_{\text{th},k} \frac{\partial \sigma}{\partial p_j} E^2 d\Omega dt \\ &- \int_{t_s}^{t_f} \int_{\Omega} -\operatorname{grad} (w_{\text{th},k}) \cdot \frac{\partial \lambda}{\partial p_j} \operatorname{grad} (\theta) d\Omega dt \\ &- \int_{\Omega} \operatorname{grad} (w_{\text{el},k}) \cdot \frac{d\mathbf{D}}{dp_j} d\Omega \Big|_{t=t_s} \\ &+ \int_{\Omega} w_{\text{th},k} \left(\frac{\partial c_V}{\partial p_j} + \frac{\partial c_V}{\partial \theta} \frac{d\theta}{dp_j} \right) \theta d\Omega \Big|_{t=t_s} \\ &+ \int_{\Omega} w_{\text{th},k} c_V \frac{d\theta}{dp_j} d\Omega \Big|_{t=t_s}, \end{aligned} \quad (13)$$

where the integrals evaluated at $t = 0$ are computed by differentiating the initial conditions (2d) and (3d). Since the adjoint problem (11) and (12) is independent of the choice of p_j , the same test functions, $w_{\text{el},k}$ and $w_{\text{th},k}$, can be used to compute the derivative of G_k with respect to any parameter. Hence, the AVM requires the solution of only one additional coupled linear system of PDEs per QoI independently of the number of parameters N_P .

3.2.1 Discretization in Space and Time

The electric scalar potential and the temperature are discretized in space according to (4a) and (4b), respectively. Furthermore, the following spatial discretizations are applied:

$$\frac{d\phi}{dp_j}(\mathbf{r}) \approx \sum_r u'_r(t) N_r(\mathbf{r}); \quad (14a)$$

$$\frac{d\theta}{dp_j}(\mathbf{r}) \approx \sum_r v'_r(t) N_r(\mathbf{r}); \quad (14b)$$

$$w_{\text{el},k}(\mathbf{r}) \approx \sum_r w_{\text{el},j}(t) N_r(\mathbf{r}); \quad (14c)$$

$$w_{\text{th},k}(\mathbf{r}) \approx \sum_r w_{\text{th},j}(t) N_r(\mathbf{r}). \quad (14d)$$

The semi-discrete counterpart of the adjoint formulation, (11) and (12), reads

$$-K_{\bar{\varepsilon}_d} \frac{\partial}{\partial t} \mathbf{w}_{\text{el},k} + K_{\bar{\sigma}_d} \mathbf{w}_{\text{el},k} - \mathbf{A}_{J+\bar{\sigma}_d}^T \mathbf{E} \mathbf{w}_{\text{th},k} = \mathbf{x}_{\text{el}}; \quad (15a)$$

$$\begin{aligned} \mathbf{A}_{\frac{\partial \varepsilon}{\partial \theta}} \mathbf{E} \frac{\partial}{\partial t} \mathbf{w}_{\text{el},k} - \mathbf{A}_{\frac{\partial \sigma}{\partial \theta}} \mathbf{E} \mathbf{w}_{\text{el},k} - \mathbf{M}_{c_v + \frac{\partial c_v}{\partial \theta} \theta} \frac{\partial}{\partial t} \mathbf{w}_{\text{th},k} \\ + \left(K_\lambda - \mathbf{A}_{-\frac{\partial \lambda}{\partial \theta} \text{grad}(\theta)} - \mathbf{M}_{\frac{\partial \sigma}{\partial \theta} E^2} \right) \mathbf{w}_{\text{th},k} = \mathbf{x}_{\text{th}}, \end{aligned} \quad (15b)$$

with

$$[\mathbf{A}_{(\cdot)}]_{rs} = \int_{\Omega} (\cdot) \cdot \text{grad}(N_s) N_r \, d\Omega; \quad (16a)$$

$$[\mathbf{x}_{\text{el}}]_j = \int_{\Omega} \frac{\partial g_k}{\partial u_j} \, d\Omega; \quad (16b)$$

$$[\mathbf{x}_{\text{th}}]_j = \int_{\Omega} \frac{\partial g_k}{\partial v_j} \, d\Omega. \quad (16c)$$

The adjoint problem is also implemented in *Pyrit*. A multi-rate coupling scheme with implicit Euler time-stepping is performed. Since the adjoint problem provides terminal conditions instead of initial conditions (see (11d), (12d)), the time-stepping is performed backwards in time. The coupling between (15a) and (15b) is resolved using the successive substitution method. The semi-discrete counterpart of (13) is given by

$$\begin{aligned} \frac{dG_k}{dp_j}(\mathbf{p}_0) &= \int_0^{t_f} \int_{\Omega} \frac{\partial g}{\partial p_j} \, d\Omega dt \\ &\quad - \int_0^{t_f} \mathbf{u}^T K_{\frac{\partial \sigma}{\partial p_j}} \mathbf{w}_{\text{el},k} \, dt \\ &\quad + \int_0^{t_f} \mathbf{u}^T K_{\frac{\partial \varepsilon}{\partial p_j}} \frac{\partial}{\partial t} \mathbf{w}_{\text{el},k} \, dt \\ &\quad + \int_0^{t_f} \mathbf{v}^T \mathbf{M}_{\frac{\partial c_v}{\partial p_j}} \frac{\partial}{\partial t} \mathbf{w}_{\text{th},k} \, dt \\ &\quad + \int_0^{t_f} \frac{\partial}{\partial t} \mathbf{w}_{\text{th},k}^T \mathbf{s} K_{\frac{\partial \sigma}{\partial p_j} E^2} \, dt \\ &\quad + \int_0^{t_f} -\mathbf{v}^T K_{\frac{\partial \lambda}{\partial p_j}} \mathbf{w}_{\text{th},k} \, dt \\ &\quad + \mathbf{u}^T K_{\frac{\partial \varepsilon}{\partial p_j}} \mathbf{w}_{\text{el},k} \Big|_{t=t_s} + (\mathbf{u}')^T K_{\bar{\varepsilon}_d} \mathbf{w}_{\text{el},k} \Big|_{t=t_s} \end{aligned}$$

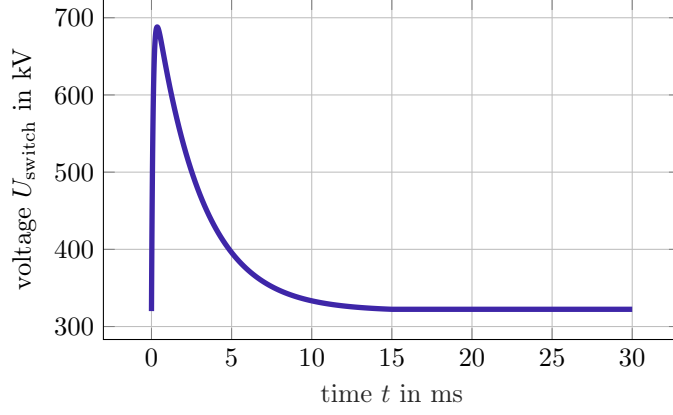


Figure 4: The switching impulse over the simulated time span $[0, 30 \text{ ms}]$.

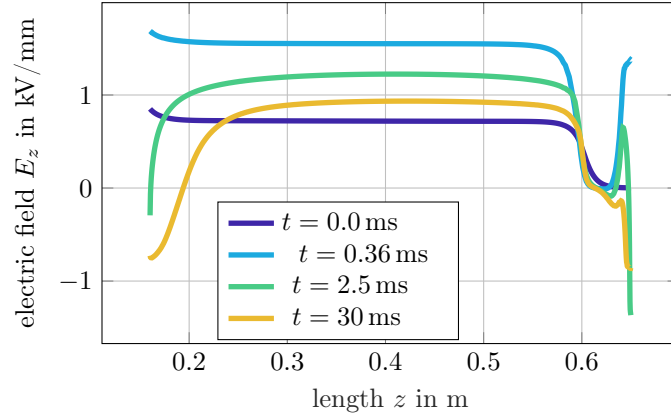


Figure 5: The tangential electric field strength, E_z , along the interface of the XLPE and the FGM (red line in Fig. 1) for different time instances.

$$\begin{aligned}
& + \mathbf{u}^T K_{\frac{\partial \varepsilon}{\partial \theta} \frac{dT}{dp}} \mathbf{w}_{\text{el}, \mathbf{k}} \Big|_{t=t_s} \\
& + \mathbf{v}^T \mathbf{M}_{\frac{\partial c_V}{\partial p_j} + \frac{\partial c_V}{\partial T} \frac{dT}{dp_j}} \mathbf{w}_{\text{th}, \mathbf{k}} \Big|_{t=t_s} \\
& + (\mathbf{v}')^T \mathbf{M}_{c_V} \mathbf{w}_{\text{th}, \mathbf{k}} \Big|_{t=t_s}
\end{aligned} \tag{17}$$

4 Simulation Studies

In this section, the AVM presented in the previous section is validated. The method is applied to the 320 kV cable joint model and the results are compared to results obtained via the DSM.

The cable joint is investigated during a switching overvoltage event, which is defined according [24, 25] as

$$U_{\text{switch}}(t) = U_{\text{DC}} + \hat{U} \frac{\tau_2}{\tau_2 - \tau_1} \left(\exp\left(-\frac{t}{\tau_2}\right) - \exp\left(-\frac{t}{\tau_1}\right) \right), \tag{18}$$

with $U_{\text{DC}} = 320 \text{ kV}$, $\hat{U} = 1.15 U_{\text{DC}} = 368 \text{ kV}$ and the constants $\tau_1 = \frac{250}{2.41} \mu\text{s}$ and $\tau_2 = \frac{2500}{0.87} \mu\text{s}$. The impulse over the simulated time span $[t_s, t_f] = [0, 30 \text{ ms}]$ is shown in Fig. 4. Figure 5 shows the tangential electric field strength along the interface between the XLPE and the FGM for several time instances. The Joule heat is 35.6 J and no significant temperature rise is observed.

The validation is performed by investigating the sensitivity of the Joule heat with respect to the material parameters of the FGM, i.e. p_1 to p_5 of (1). This is motivated by the findings of [9] and [5], where it has been demonstrated that inappropriate choices for p_1 to p_5 can result in a substantial

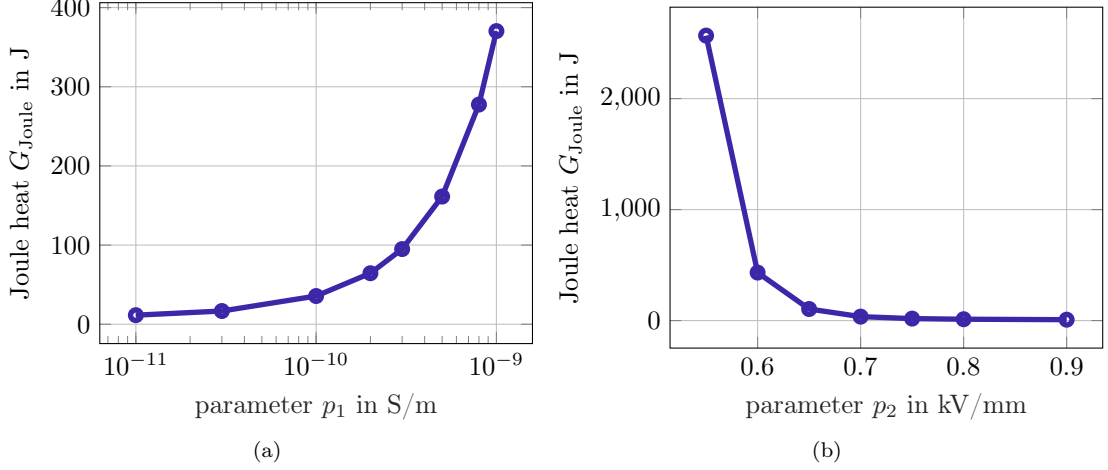


Figure 6: Joule heat as an exemplary QoI for (a) different values of p_1 and (b) different values of p_2 .

elevation of the Joule heat and consequently a significant temperature increase (see Fig. 6). To apply the AVM, the Joule heat is written in terms of a functional g_{Joule} ,

$$G_{\text{Joule}}(\phi, T, \mathbf{p}) = \int_{\Omega} \int_{t_s}^{t_f} g_{\text{Joule}}(\phi, T, \mathbf{r}, t, \mathbf{p}) \, d\Omega \, dt = \int_{\Omega} \int_{t_s}^{t_f} \mathbf{J} \cdot \mathbf{E} \, d\Omega \, dt. \quad (19)$$

Note that this integral notation does not restrict the choice of QoIs. QoIs that may not inherently be expressed as an integral can be effectively represented using Dirac delta functions, δ , within the integral expression. For example, the temperature $\theta(\mathbf{r}_{\text{QoI}}, t_{\text{QoI}})$ at a particular position, \mathbf{r}_{QoI} , and time instance, t_{QoI} , reads in integral notation:

$$G_{\theta(\mathbf{r}_{\text{QoI}}, t_{\text{QoI}})}(\phi, T, \mathbf{p}) = \int_{\Omega} \int_{t_s}^{t_f} \theta(\mathbf{r}, t) \delta(\mathbf{r} - \mathbf{r}_{\text{QoI}}) \delta(t - t_{\text{QoI}}) \, d\Omega \, dt. \quad (20)$$

For more information on QoIs that are evaluated at specific points in space or time and the numeric implications, see [15]. The QoI-dependent parts of the FE formulation are defined by

$$\int_{\Omega} \frac{\partial g_{\text{Joule}}}{\partial p_j} \, d\Omega \approx \mathbf{u}^T \mathbf{K}_{\frac{\partial \sigma}{\partial p}} \mathbf{u}, \quad (21a)$$

$$\mathbf{x}_{\text{el}} = \mathbf{u}^T (\mathbf{K}_{\sigma} + \mathbf{K}_{\bar{\sigma}_d}), \quad (21b)$$

$$\mathbf{x}_{\text{th}} = \mathbf{s}_{\frac{\partial \sigma}{\partial T}} E^2. \quad (21c)$$

The results are collected in Table 1. The sensitivities are both positive and negative and their absolute values vary substantially. Comparing the absolute value of the sensitivity to p_1 and p_2 , respectively, indicates that the QoI is much more sensitive to changes in p_1 compared to p_2 . However, the comparison of the derivatives should take the absolute value of the parameters into account. This can be done for example by using a first order Taylor series approximation of the QoI's dependence on the parameters,

$$G_{\text{Joule}}(p_j) \approx G_{\text{Joule}}(p_{0,j}) + \frac{dG_{\text{Joule}}}{dp_j}(p_{0,j}) \Delta p_j, \quad j = 1, \dots, 5,$$

where $\Delta p_j = p_j - p_{0,j}$ is the perturbation of the j -th parameter. The Taylor series can be used to estimate the relative change of a QoI that occurs for an increase of a parameter $\Delta p_j = 1\% p_{0,j}$, i.e.

$$\Delta G_{1\%,j} := \frac{\Delta G_{\text{Joule}}}{G_{\text{Joule}}(p_{0,j})} \approx \frac{dG_{\text{Joule}}}{dp_j}(p_{0,j}) \frac{1\% p_{0,j}}{G_{\text{Joule}}(p_{0,j})}, \quad (22)$$

with $\Delta G_{\text{Joule}} = G_{\text{Joule}}(p_{0,j} + \Delta p_j) - G_{\text{Joule}}(p_{0,j})$. The normalized sensitivities are brought together in Table 2. Comparing the normalized value of the derivatives to p_1 and p_2 now shows that the QoI actually is much more sensitive towards relatively small changes in p_2 compared to p_1 (see Fig. 7a and

Table 1: Sensitivities of the Joule heat with respect to the parameters p_1 to p_5 of the nonlinear FGM conductivity defined by (1).

Parameter p_j	Value $p_{0,j}$	Derivative $\frac{dG}{dp_j}(\mathbf{p}_0)$
p_1	1.0e-10 S/m	2.76e+11 kJ/(S/m)
p_2	0.70 kV/mm	-6.28e-4 kJ/(kV/mm)
p_3	2.4kV/mm	2.38e-8 kJ/(kV/mm)
p_4	1900	1.65e+2 kJ
p_5	3700	1.01e+2 kJ

Table 2: Normalized sensitivities according to (22) of the Joule heat with respect to the parameters p_1 to p_5 of the nonlinear FGM conductivity defined by (1).

Parameter p_j	Normalized sensitivity $\Delta G_{1\%,j}$
p_1	0.780 %
p_2	-12.4 %
p_3	1.61e-3 %
p_4	0.870 %
p_5	1.06 %

Fig. 7b). Finally, the adjoint formulation (11) and (12) is validated by comparing the sensitivities of the Joule heat obtained by the AVM to two reference solutions. The first reference solution is obtained by the commercial simulation software COMSOL Multiphysics® and the second reference solution is computed using the DSM which is also implemented in *Pyrit*. Fig. 8 shows that the results agree for all parameters. Hence, the method is successfully validated.

Figure 9 investigates the convergence behavior of the AVM. Figure 9a shows that the relative error, ϵ_{rel} , of the sensitivity $\frac{dG}{dp_2}(\mathbf{p}_0)$ of the Joule losses to p_2 converges quadratically with respect to the maximum edge length inside the 2D triangular mesh. In order to achieve a relative error below one 1%, mesh consisting of 24722 nodes and 52544 elements is selected for all further computations.

Figure 9b shows the relative error, ϵ_{rel} , of the sensitivity $\frac{dG}{dp_1}(\mathbf{p}_0)$ of the Joule losses to p_2 with respect to the time step size. As expected for the implicit Euler method, the relative error converges quadratically with respect to the time step size. With a maximum step size of $\Delta t_{\text{max}} = 0.56$ ms, a relative error below 0.1 % can be achieved. It furthermore shows the convergence of the sensitivity with respect to the maximum thermal time step, $\Delta t_{\text{th,max}}$, while the maximum electric time step is fixed at $\Delta t_{\text{el,max}} = 0.56$ ms. The thermal time step can be chosen approximately 5.4 times larger than the electric time step, demonstrating the benefits of a multi-rate time-integration approach. The AVM is, thus, successfully validated, which is an important step towards the optimization of FGMs in HVDC cable joints.

5 Conclusion

The adjoint variable method is an efficient approach for computing sensitivities of quantities of interest with respect to a large number of the design parameters. In this work, the adjoint variable method is formulated for coupled transient electrothermal problems with nonlinear media and implemented in the finite element framework *Pyrit*. The method is applied to the numerically challenging example of a 320 kV cable joint specimen under switching operation. The computed sensitivities are compared to results obtained by the direct sensitivity method and the method is successfully validated. The convergence of the adjoint variable method is discussed and the benefits of a multi-rate time-integration approach are demonstrated. This is an important step towards efficient and systematic design and optimization of high voltage direct current cable joints.

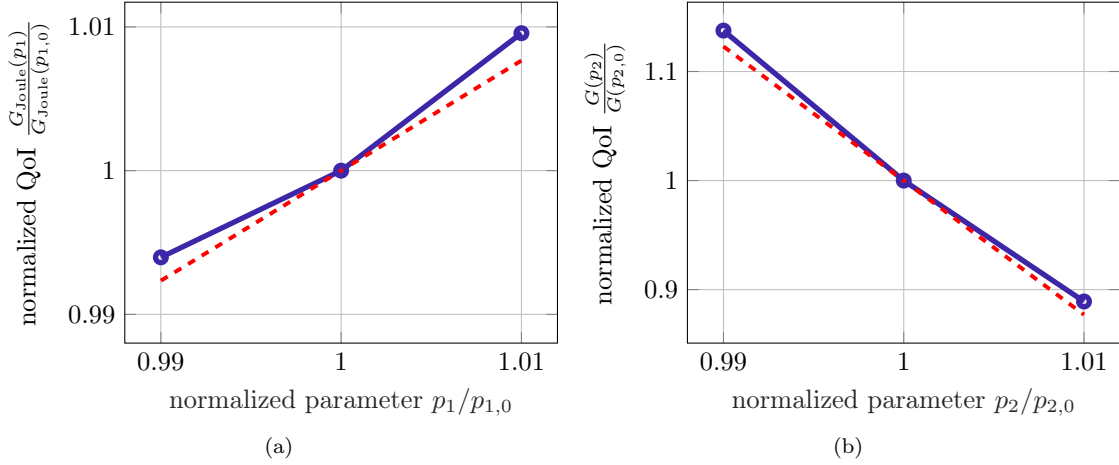


Figure 7: The QoI, i.e. the Joule heat, for different values of (a) p_1 and (b) p_2 . The red lines indicate the tangent slope computed by the AVM.

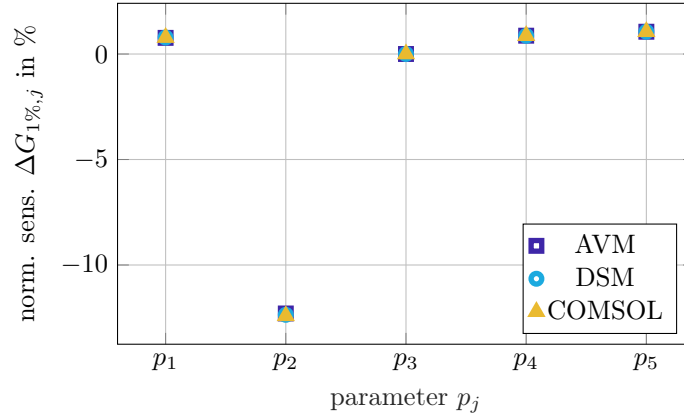


Figure 8: Comparison of the sensitivities of the Joule heat computed by the AVM and DSM, respectively.

6 Acknowledgements

The authors thank Rashid Hussain for providing the simulation model and material characteristics published in [5]. This work is supported by the DFG project 510839159, the joint DFG/FWF Collaborative Research Centre CREATOR (CRC-TRR361/F90) and the Graduate School Computational Engineering at the Technische Universität Darmstadt. Yvonne Späc-Leigsnering holds an Athene Young Investigator Fellowship of the Technische Universität Darmstadt.

References

- [1] Cigré Working Group D1.56. *Field grading in electrical insulation systems*. Technical Brochure TB794. Conseil international des grands réseaux électriques, 2020.
- [2] G. Chen, M. Hao, Z. Xu, A. Vaughan, J. Cao, and H. Wang. “Review of high voltage direct current cables”. In: *CSEE J. Power Energy Syst.* 1.2 (July 24, 2015), pp. 9–21. DOI: 10.17775/CSEEJPES.2015.00015.
- [3] H. Ghorbani, M. Jeroense, C.-O. Olsson, and M. Saltzer. “HVDC cable systems – highlighting extruded technology”. In: *IEEE Trans. Power Deliv.* 29.1 (2014), pp. 414–421. DOI: 10.1109/TPWRD.2013.2278717.
- [4] C. Jörgens and M. Clemens. “A review about the modeling and simulation of electro-quasistatic fields in HVDC cable systems”. In: *Energies* 13.19 (Oct. 2020), p. 5189. DOI: 10.3390/en13195189.
- [5] R. Hussain and V. Hinrichsen. “Simulation of thermal behavior of a 320 kV HVDC cable joint with nonlinear resistive field grading under impulse voltage stress”. In: *CIGRÉ Winnipeg 2017 Colloquium*. 2017.
- [6] M. Secklehner, R. Hussain, and V. Hinrichsen. “Tailoring of new field grading materials for HVDC systems”. In: *13th International Electrical Insulation Conference (INSUCON 2017)*. May 2017. DOI: 10.23919/insucon.2017.8097174.

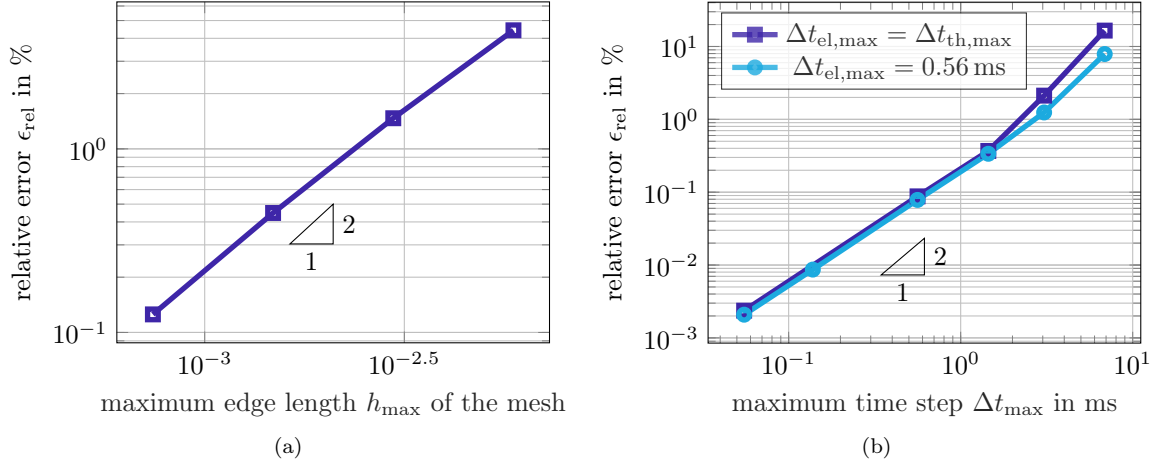


Figure 9: Convergence of the sensitivity $\frac{dG}{dp_2}$ of the Joule heat to p_2 with respect to (a) the mesh size and (b) the time step size.

- [7] J. Bauer, A. Claudi, S. Kornhuber, S. Kühnel, J. Lambrecht, and S. Wels. “Silicon-Gel-Compound für die Nichtlinear-Resistive Feldsteuerung — zur Technischen Anwendung und Auslegung des Isoliersystems”. In: *Fachtagung Hochspannungstechnik 2020 (VDE ETG)*. Berlin, Germany, Nov. 2020, pp. 163–168.
- [8] C. Jörgens and M. Clemens. “Comparison of two electro-quasistatic field formulations for the computation of electric field and space charges in HVDC cable systems”. In: *22nd Conference on the Computation of Electromagnetic Fields (COMPUMAG 2019)*. Ed. by Z. Ren. International Compumag Society. Paris, France, July 2019. DOI: 10.1109/compumag45669.2019.9032818.
- [9] Y. Späck-Leigsnering, G. Ruppert, E. Gjonaj, H. De Gersem, and M. Koch. “Towards Electrothermal Optimization of a HVDC Cable Joint Based on Field Simulation”. In: *Energies* 14.10 (May 2021), p. 2848. DOI: 10.3390/en14102848.
- [10] I. G. Ion et al. “Deterministic Optimization Methods and Finite Element Analysis With Affine Decomposition and Design Elements”. In: *Electr. Eng.* 100.4 (Dec. 2018), pp. 2635–2647. DOI: 10.1007/s00202-018-0716-6.
- [11] S. Li and L. Petzold. “Adjoint sensitivity analysis for time-dependent partial differential equations with adaptive mesh refinement”. In: *J. Comp. Phys.* 198.1 (July 2004), pp. 310–325. DOI: 10.1016/j.jcp.2003.01.001.
- [12] N. Nikolova, J. Bandler, and M. Bakr. “Adjoint Techniques for Sensitivity Analysis in High-Frequency Structure CAD”. In: *IEEE Trans. Microw. Theor. Tech.* 52.1 (Jan. 2004), pp. 403–419. DOI: 10.1109/tmtt.2003.820905.
- [13] Y. Cao, S. Li, L. Petzold, and R. Serban. “Adjoint sensitivity analysis for differential-algebraic equations: The adjoint DAE system and its numerical solution”. In: *SIAM J. Sci. Comput.* 24.3 (2003), pp. 1076–1089. DOI: 10.1137/S1064827501380630.
- [14] D. Zhang, F. Kasolis, and M. Clemens. “Topology Optimization for a Station Class Surge Arrester”. In: *The 12th International Symposium on Electric and Magnetic Fields (EMF 2021)*. 2021.
- [15] M. G. Ruppert, Y. Späck-Leigsnering, J. Buschbaum, and H. De Gersem. “Adjoint Variable Method for Transient Nonlinear Electroquasistatic Problems”. In: *Electr. Eng.* 105 (Apr. 2023), pp. 2319–2325. DOI: 10.1007/s00202-023-01797-4.
- [16] M. G. Ruppert, Y. Späck-Leigsnering, J. Buschbaum, M. Koch, and H. De Gersem. “Efficient Sensitivity Calculation for Insulation Systems in HVDC Cable Joints”. In: *27th Nordic Insulation Symposium on Materials, Components and Diagnostics (Trondheim)*. June 2022.
- [17] R. Hussain. “Electrothermal FEM simulation of relevant test conditions of a 525 kV HVDC cable joint including nonlinear field grading material”. In: *Jicable’23: 11th International Conference on Insulated Power Cables (Lyon)*. June 2023.
- [18] M. Koch, J. Hohloch, I. Wirth, S. Sturm, M. H. Zink, and A. Küchler. “Experimental and simulative analysis of the thermal behavior of high voltage cable joints”. In: *VDE ETG – Fachtagung Hochspannungstechnik 2018*. Nov. 2018.
- [19] T. T. N. Vu, G. Teyssedre, and S. Le Roy. “Electric field distribution in HVDC cable joint in non-stationary conditions”. In: *Energies* 14.17 (Aug. 30, 2021), p. 5401. DOI: 10.3390/en14175401.
- [20] J. Bundschuh, M. G. Ruppert, and Y. Späck-Leigsnering. “Pyrit: A finite element based field simulation software written in Python”. In: *COMPEL* 42 (Sept. 2023), pp. 1007–1020. DOI: 10.1108/compel-01-2023-0013.
- [21] M. Saltzer, T. Christen, T. Sörqvist, and M. Jeroense. “Electro-thermal simulations of HVDC cable joints”. In: *Proceedings of the ETG Workshop Feldsteuernde Isoliersysteme*. Berlin, Offenbach: VDE-Verlag, Nov. 2011.
- [22] T. Schierz and M. Arnold. “Stabilized overlapping modular time integration of coupled differential-algebraic equations”. In: *Applied Numerical Mathematics* 62 (Oct. 2012), pp. 1491–1502. DOI: 10.1016/j.apnum.2012.06.020.

- [23] H. De Gersem, I. Munteanu, and T. Weiland. “Construction of Differential Material Matrices for the Orthogonal Finite-Integration Technique With Nonlinear Materials”. In: *IEEE Trans. Magn.* 44.6 (June 2008), pp. 710–713. doi: 10.1109/TMAG.2007.915819.
- [24] A. Küchler. *High Voltage Engineering: Fundamentals - Technology - Applications*. 1st ed. VDI-Buch. Berlin, Heidelberg, 2018. doi: 10.1007/978-3-642-11993-4.
- [25] Cigré Working Group B1.32. *Recommendations for Testing DC Extruded Cable Systems for Power Transmission at a Rated Voltage up to 500 kV*. Technical Brochure TB496. Conseil international des grands réseaux électriques, 2012.